

Article Title: AI-based data corrections for attenuation and scatter in PET and SPECT

Authors:

Alan B. McMillan, PhD (corresponding author)
Associate Professor, Department of Radiology, University of Wisconsin, Madison, WI, USA
3252 Clinical Science Center, 600 Highland Ave, Madison, WI 53792
amcmillan@uwhealth.org, @alan_b_mcmillan

Tyler J. Bradshaw, PhD
Associate Scientist, Department of Radiology, University of Wisconsin, Madison, WI, USA
3252 Clinical Science Center, 600 Highland Ave, Madison, WI 53792
tbradshaw@wisc.edu, @tybradshaw11

Corresponding Author: Alan B McMillan, PhD

Disclosure Statement: The Dept of Radiology at the University of Wisconsin receives support from GE Healthcare.

Funding Acknowledgement: Research reported in this publication was supported by the National Institute of Biomedical Imaging and Bioengineering of the National Institutes of Health under award number R01EB026708.

Key Words: Artificial intelligence, deep learning, attenuation correction, scatter correction, PET SPECT

Key Points:

- Promising AI techniques are being used to improve attenuation and scatter correction for PET and SPECT imaging.
- AI-based attenuation correction can provide high quality synthetic CTs from other available images such as MRI or uncorrected PET images to improve the capability of PET and SPECT.
- AI-based scatter correction can accelerate PET reconstruction.
- AI methods can be used to estimate both attenuation and scatter simultaneously.

Synopsis: This article reviews the use of artificial intelligence-based methods for improving attenuation and/or scatter correction in PET and SPECT imaging.

Abstract: Recent developments in artificial intelligence technology have enabled new developments that can improve attenuation and scatter correction in PET and SPECT. These technologies will enable the use of accurate and quantitative imaging without the need to acquire a CT image, greatly expanding the capability of PET/MRI, PET-only, and SPECT-only scanners. The use of AI to aid in scatter correction will lead to improvements in image reconstruction speed, and improve patient throughput. This paper outlines the use of these new tools, surveys contemporary implementation, and discusses their limitations.

Introduction

Both PET and SPECT reconstructions require several corrections in order to yield high quality quantitative images. These corrections include: correction for random coincidences, detector dead-time, detector normalization, scattered coincidences (commonly referred to as scatter correction), and attenuation¹. For the correction of scatter and attenuation, the tendency of electrons within the underlying tissue to induce Compton scattering due to electron interaction of PET or SPECT photons. This results in undetected annihilation events (attenuation) or the detection of anomalous coincidences (scatter). The likelihood of a photon interacting with a medium increases with both the distance traveled as well as the electron density of the underlying tissue and material through which the photons travel. Therefore, in order to accurately estimate attenuation and scatter, an additional image that provides linear attenuation coefficients of the material is needed. Historically this has necessitated the use of an external radioactive source to obtain transmission images on a PET system², and more recently has relied upon the use of CT to obtain this information for PET/CT and SPECT/CT. The more recent development of PET/MR has complicated this matter, where MR images are not routinely capable of identifying bone with positive contrast, making a direct conversion of MR data into a linear attenuation coefficients challenging¹.

Scattered coincidences typically account for 30-50% of the detected coincidence events in a PET scan. Scatter correction algorithms, such as the single scatter simulation method, require knowledge of the local activity concentration in addition to the attenuation coefficients of the object in order to estimate the likelihood of scattered coincidences. As the local activity concentration is only known after image reconstruction with scatter correction, iterative methods are typically required and can be time consuming to compute. While a full review of scatter corrections is not possible here, several reviews are dedicated to this problem³⁻⁵.

In the past several years there has been a great effort to develop algorithms that utilize artificial intelligence (AI), that is, machine learning and deep learning techniques, to aid in the processing and reconstruction of medical imaging data. These techniques hold much promise in solving some of the quantitative challenges related to scatter and attenuation, particularly when additional transmission or CT imaging is unavailable or undesired in the attempt to reduce patient ionizing radiation exposure, or when

patient motion degrades the effectiveness of the CT image, or for other reasons. Particularly in the development of PET/MR systems, where CT is not possible, there has been a particularly intense focus on the development of machine learning-based techniques that have demonstrated strong preliminary performance. AI-based approaches, unlike other algorithms, “learn” to perform the task at hand, which in this case is the production of a CT-like image. AI techniques use the concept of supervised learning, where examples of input images, such as an MRI scan, are paired with training labels that represent the desired output image, such as a CT. Through a complex process of backpropagation and iterative training^{6,7}, these algorithms are able to learn the relationships between features of the input data and the desired output. More recently, deep learning-based techniques, and in particular convolutional neural networks, have received substantial interest compared to more conventional machine learning-based techniques.

AI-based Methods

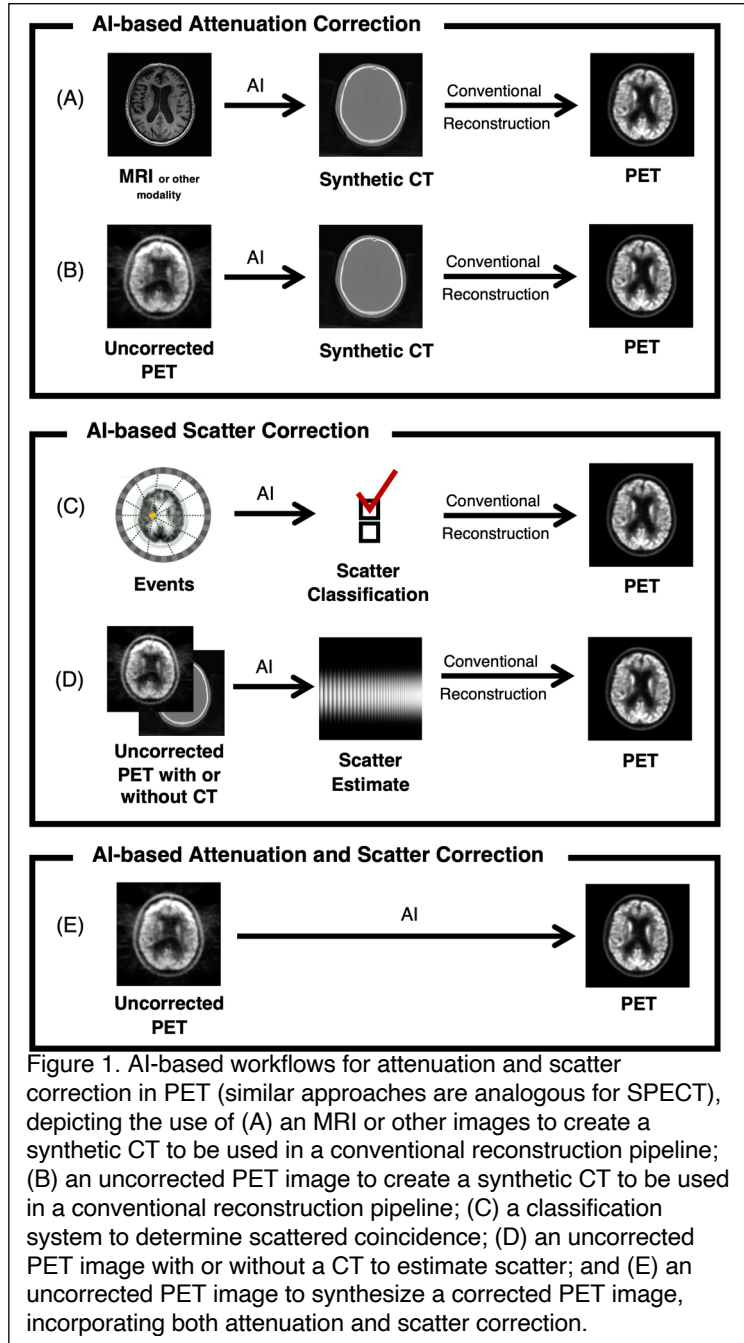
A block diagram of an AI-based workflow for AI-based attenuation and/or scatter correction is shown in Figure 1. Here an MR input image is paired with a CT image from the same patient to create a database of image pairs. Upon successful spatial registration of these two datasets, a deep learning network is used to train a model that synthesizes a CT-like image from only an MRI input. Once fully trained, the model is able to yield synthetic CT images that would be appropriate inputs into a conventional PET reconstruction pipeline. The performance of any given AI-based approach is going to depend on the type and structure of the underlying model that is utilized. While numerous types of models or networks could be used for a given application, the literature suggests that several types of specific model architectures are particularly effective. For example, most AI-based approaches utilize convolutional neural networks (CNNs). CNNs consist of multiple layers of synthetic neurons that learn the convolution kernels and sample weights to encode various features in both the input and desired output images^{6,7}. There are many CNN-based architectures that have been developed, but two specific architectures have been the most studied for attenuation and scatter correction, shown in Figure 2. The

first is the UNet, which is a nearly ubiquitous in its application to image processing in a wide range of fields⁷.

This model utilizes a combination of essentially two models, one to encode the features of the input image, and another to decode the learned features into the desired output image. A key feature of the UNet is the sharing of learned features between encoding and decoding side of the network, which improves model performance.

Another popular model structure is the generative adversarial network (GAN). A GAN consists of two separate models, one model as a generator, which is used to synthesize the output, and second model, a discriminator, which is used to determine the quality of the

synthesized output from the generator⁸. Essentially, the generator is trained such that it can create a synthesized image (e.g., a synthetic CT image) for which the discriminator cannot determine whether the generated image is real or fake. The discriminator learns from real examples and is trained to identify the fake images from the generator. The advantage of GAN-based approaches is that they can produce more realistic looking outputs. Some types of GANs do not require spatially-registered input-output pairs, which



can be challenging to acquire, thus greatly reducing the burden of having paired datasets with multi-modality image registration.

Evaluation Metrics

The performance of a trained algorithm in synthesizing CT images is typically evaluated utilizing various metrics that compare the model's synthetic CT image to the original CT from the same patient. Common metrics to assess quality include root mean square error (RMSE), mean absolute error (MAE), structural similarity index (SSIM), peak signal to noise ratio (PSNR), and Dice coefficient (DC). Additionally, the PET or

SPECT images reconstructed using the synthetic CT can be compared to the same image reconstructed using the ground truth CT. The final bias in the reconstructed image can then be quantified. Each of these metrics have their own relative strengths and weaknesses and thus the evaluation of a single model's performance should utilize multiple metrics. There exist no standard approaches for the assessment of attenuation and scatter algorithms, so investigators typically report using one or more of the aforementioned metrics. Unfortunately, this can make it difficult to compare results between different approaches.

RMSE is a measure of the square root of the average squared difference between the synthesized CT and the original CT calculated for each voxel in the image, using the following equation:

$$RMSE(\hat{y}, y) = \sqrt{\frac{\sum(\hat{y}-y)^2}{n}} \quad (1)$$

, where \hat{y} is the synthesized CT, y is the original CT, and n is the number of voxels. RMSE values are often calculated separately for soft tissue regions and bone and have units that match the original image, in this case Hounsfield units. High performing approaches typically have RMSE values of 100 HU or less.

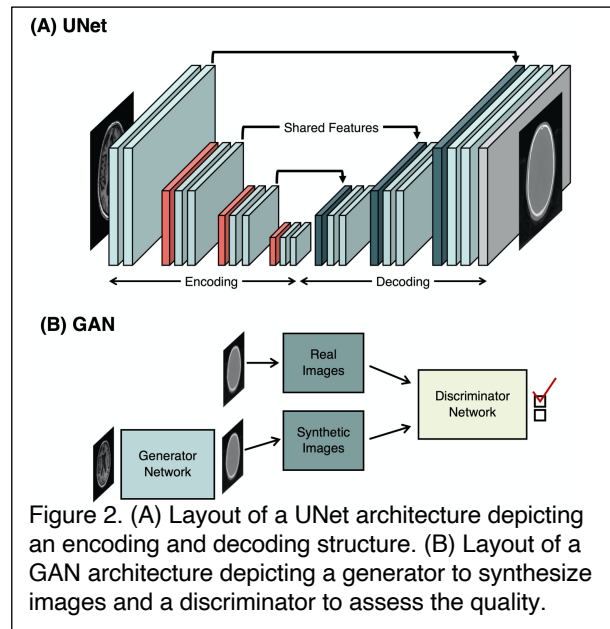


Figure 2. (A) Layout of a UNet architecture depicting an encoding and decoding structure. (B) Layout of a GAN architecture depicting a generator to synthesize images and a discriminator to assess the quality.

MAE is similar to the RMSE except that it is the absolute error rather than the squared error as calculated using the following equation:

$$MAE(\hat{y}, y) = \sqrt{\frac{\sum |\hat{y} - y|}{n}} \quad (2)$$

. MAE also yields error in units that match the original image. One limitation of the MAE approach is that if errors are centered around zero, the values of MAE may be much smaller than RMSE. Both RMSE and MAE can be sensitive to the cropping of the images: if images contain large amounts of surrounding air, this can have the effect of decreasing the average error, as models can often predict surrounding air with near perfect accuracy.

SSIM is another measure of the image quality widely used throughout the computer vision literature. SSIM yields a metric on a scale that ranges between -1 to 1, where an SSIM 1 represents a perfect recovery of the original image. SSIM can be calculated using the following equations:

$$SSIM(\hat{y}, y) = \frac{(2\mu_{\hat{y}}\mu_y + c_1)(2\sigma_{\hat{y}y} + c_2)}{(\mu_{\hat{y}}^2 + \mu_y^2 + c_1)(\sigma_{\hat{y}}^2 + \sigma_y^2 + c_2)} \quad (2)$$

$$c_1 = (K_1L)^2$$

$$c_2 = (K_2L)^2$$

, where $\mu_{\hat{y}}$, μ_y , $\sigma_{\hat{y}}^2$, σ_y^2 , $\sigma_{\hat{y}y}$ are the average, variance, and covariance of \hat{y} and y , respectively. K_1 and K_2 are constants equal to 0.01 and 0.03. L is equal to the dynamic range (i.e., the range from the smallest to largest pixel value) in the image.

PSNR is a measure of relative power of the relative difference or noise in an image compared to its reference, and can be calculated using the following equation:

$$PSNR = 10\log_{10}(L^2/MSE) \quad (3)$$

DC is measure of overlap between discrete regions of a segmented image, where a coefficient of 1 means perfect overlap. This metric is frequently used to determine the ability of AI approaches to estimate specific regions such as air, soft tissue, and bone. DC can be calculated using the following equation:

$$\text{Dice Coefficient} = (2 * TP) / (2 * TP + FN + FP) \quad (4)$$

, where TP is the number of true positives, FN is the number of false negatives, and FP is the number of false positives in a segmented image relative to the reference. DC is often used to assess the quality of bone estimate in brain attenuation correction approaches. For studies in the brain, DC of 0.8 or greater in bone typically identifies a very good performing synthetic CT approach.

The end goal of CT synthesis is to use the CT for attenuation and scatter correction and create nuclear medicine images with minimum bias. Thus reconstruction bias is an important metric that compares the end result of a given attenuation or scatter correction approach to the conventional approach. Bias is typically represented as a percentage of error within a given region or over the entire image. Reconstruction image is typically calculated as follows:

$$Bias(\hat{y}, y) = \frac{y - \hat{y}}{y} \times 100\% \quad (5)$$

Reconstruction bias averaged over the entire image can hide errors or biases occurring in small regions of high importance, such as tumors. These regions should be quantified and compared.

AI-Based Attenuation Correction

For AI-based attenuation correction methods, the AI algorithm synthesizes a CT-like image that can then be used in place of a CT within a conventional reconstruction pipeline. The input for the algorithm is typically an MR image (as used for simultaneous PET/MR imaging), as shown in Figure 1A, or the underlying uncorrected PET or SPECT image itself, as shown in Figure 1B. The goal of the AI algorithm is not necessarily to create a diagnostic image, but one that is sufficiently realistic image and minimizes the reconstruction bias in the final image. One shortcoming of most published AI approaches is that the models are typically trained to be tuned to identifying one anatomical region, such as the brain, chest, or pelvis and are generally not applicable to the whole body. While this does not necessarily limit these algorithms for their intended use, it does require that separate approaches be developed for each individual body part. As the feasibility of anatomic-specific algorithms for attenuation correction has already been well established, future approaches should focus on whole-body corrections, such that a uniform approach can be used regardless of the anatomy being scanned.

Several recent reviews have compared the performance of the increasing number of AI-based approaches proposed for synthetic CT generation^{9–11}. In Table 1, we highlight several approaches evaluated in different body regions including the brain, chest, and pelvis for both PET and SPECT. Due to the rapid pace of innovation in this area, these results are likely to be soon joined by new and better performing approaches. However, these results demonstrate that high performing approaches already exist that appear to provide sufficient quantitative results without the need for the acquisition of a CT. Note that approaches that include a joint estimation of attenuation and scatter (Figure 1E) are listed in Table 3.

Application	Approach	Advance	Quantitative Comparison vs. Acquired CT	Reference
Brain perfusion SPECT	CNN	Enable correction for SPECT only scanners	PSNR 62.2 dB, SSIM 0.9995	Sakaguchi et al., 2021 ¹²
Brain PET (FDG)	CNN, UNet	Enable correction for PET only scanners	Dice coefficients of 0.80 ± 0.02 for air, 0.94 ± 0.01 for soft tissue, and 0.75 ± 0.03 for bone, MAE of 111 ± 16 HU, PET reconstruction bias $<1\%$	Liu et al., 2018 ¹³
Brain PET/MR (FDG)	CNN	Synthesize CT from T1 MRI for PET/MRI	Dice coefficient of 0.936 ± 0.011 for soft tissue, and 0.803 ± 0.021 for bone, PET reconstruction bias $-0.7\% \pm 1.1\%$	Liu et al., 2017 ¹⁴
Brain PET/MR (FDG)	CNN, GAN	Synthesize CT from T1 MRI for PET/MRI	Dice coefficient of 0.77 ± 0.07 for bone, PET reconstruction bias $<4\%$	Arabi et al., 2019 ¹⁵
Brain PET/MR (FDG)	CNN, GAN	Synthesize CT from T1 MRI for PET/MRI	Dice coefficient of 0.74 ± 0.05 for bone, PET reconstruction bias <0.025 SUV	Gong et al., 2020 ¹⁶
Brain PET/MR (FDG)	CNN, UNet	Synthesize CT from T1 MRI for PET/MRI	Dice coefficient of 0.81 ± 0.03 for bone, PET RMSE 253.5, PET reconstruction bias $<1\%$	Blanc-Durand et al., 2019 ¹⁷
Brain PET/MR (FDG)	CNN, UNet	Synthesize CT from T1 and ZTE MRI for PET/MRI	Dice coefficient of 0.86 ± 0.03 for bone, PET reconstruction bias <0.02 SUV	Gong et al., 2018 ¹⁸
Brain PET/MR (FDG)	CNN, UNet	Synthesize CT from UTE MRI for PET/MRI	Dice coefficient of 0.96 ± 0.006 for soft tissue, 0.88 ± 0.01 for bone, PET reconstruction bias $<1\%$	Jang et al., 2018 ¹⁹
Brain PET/MR (FET)	CNN, UNet	Synthesize CT from UTE MRI for PET/MRI	PET reconstruction bias $<1\%$	Ladefoged et al., 2019 ²⁰
Myocardial perfusion SPECT	CNN	Enable correction for SPECT only scanners	MAE $3.60\% \pm 0.85\%$ in whole body, $1.33\% \pm 3.80\%$ in the left ventricle	Shi et al., 2020 ²¹
Myocardial perfusion SPECT	CNN	Enable correction for SPECT only scanners	Mean segmental errors $0.49 \pm 4.35\%$, mean absolute segmental errors $3.31 \pm 2.87\%$	Yang et al., 2021 ²²
Myocardial perfusion SPECT	GAN	Enable correction for SPECT only scanners	RMSE 0.141 ± 0.0768 , PSNR 36.382 ± 3.74 dB, SSIM 0.995 ± 0.0043	Torkaman et al., 2021 ²³
Pelvis PET/MR (68Ga-PSMA)	CNN, GAN	Synthesize CT from T1 MRI for PET/MRI	PET reconstruction bias $<2.2\%$	Pozaruk et al., 2021 ²⁴
Pelvis PET/MR (FDG)	CNN	Synthesize CT from T1 and T2 MRI for PET/MRI	Dice coefficient of 0.98 ± 0.01 for soft tissue, 0.79 ± 0.03 for cortical bone, PET reconstruction bias 4.9%	Bradshaw et al., 2018 ²⁵
Pelvis PET/MR (FDG)	CNN, UNet	Synthesize CT from T1 MRI for PET/MRI	PET reconstruction bias $<4\%$	Torrado-Carvajal et al., 2019 ²⁶
Whole body PET (FDG)	CNN, GAN	Enable correction for PET only scanners	PET reconstruction bias $-0.8 \pm 8.6\%$	Armanious et al., 2020 ²⁷

In the future, AI-based approaches may even exceed the capability of existing CT approaches, for example in the case of motion, where it might not be feasible to acquire additional CT imaging due to physiological and/or bulk patient movement. It could also improve dynamic imaging over long periods (or

dual time point imaging) without needing to reacquire a CT. It appears that it may be feasible to leverage an AI-based approach to construct a motion-compensated synthetic CT or even a multi-phase CT, directly from the underlying PET or SPECT data. While there exist some potential limitations with AI-based approaches, it is likely that these approaches will gain greater clinical acceptance in the near future. Furthermore, the development of AI-based approaches for synthetic CT images to aid in attenuation correction is highly synergistic with the development of MR-only radiotherapy²⁸. In this application, the valuable soft tissue contrast of MRI is useful in the delineation of tumors, yet MRI is challenged in the direct synthesis of CT-like images. Therefore, there has also been great interest in developing synthetic CT technology using AI in the radiotherapy. Developments for both improved diagnostic imaging capability in PET and SPECT as well as for radiotherapy are expected to be mutually beneficial, as the underlying techniques and AI models are highly similar.

AI Scatter Correction

AI based approaches to scatter correction promise to increase the overall speed of image reconstruction due to the often time-consuming nature of estimating scatter correction. Additionally, AI may allow for more accurate scatter estimation, potentially replacing single scatter simulation with an AI model that approximates multi-scatter events by using training data from Monte Carlo modeling. For example as shown in Figure 1C, one proposed approach for accelerating scatter utilizes the position and energy level of each coincidence event to predict whether an event can be categorized as originating from scatter or not²⁹. Most approaches attempt to estimate the scatter profile directly from given inputs of activity as shown in Figure 1D. A summary of recent approaches to improve scatter correction (not including methods that jointly estimate scatter and attenuation) are listed in Table 2.

Application	Approach	Advance	Reference
PET	Machine learning to classify events as true or scattered coincidences	Potential for scatter correction being performed prior to imaging reconstruction	Prats et. al, 2019 ²⁹
PET	Cascade of CNNs to estimate Monte Carlo-based approach	Improved speed relative to Monte Carlo methods	Qian et. al, 2017 ³²
PET/MR	CNN to estimate single-scatter simulation (SSS)	Significant increase in reconstruction speed	Berker et. al, 2018 ³⁰
SPECT	CNN to improve filtered backprojection images to	>200x faster than Monte Carlo method	Dietze et. al, 2019 ³³

	approximate Monte Carlo-based approach		
SPECT , Y-90 bremsstrahlung imaging	CNN to estimate scatter projections	>120x faster than Monte Carlo method	Xiang et. al, 2020 ³¹

Given that attenuation information is necessary to perform scatter estimation, and both are unknown without a CT image, many recent approaches have attempted to utilize AI approaches to determine *both* attenuation and scatter, particularly using only uncorrected PET and SPECT images as inputs. The example workflow is shown in Figure 1E and a summary of these methods are listed in Table 3.

Application	Approach	Quantitative Comparison vs. Acquired CT	Reference
Brain PET (FDG, FDOFA, Flortaucipir, Flutemetamol)	CNN	PET reconstruction bias <9%	Arabi et al., 2020 ³⁴
Brain PET (FDG)	CNN, UNet	PET reconstruction bias -4.2% ± 4.3%	Yang et al., 2019 ³⁵
Whole body PET (68Ga-PSMA)	CNN	MAE 0.91 ± 0.29 SUV, SSIM 0.973 ± 0.034, PSNR 48.17 ± 2.96 dB, PET reconstruction bias -2.46% ± 10.10%	Mostafapour et al., 2021 ³⁶
Whole body PET (FDG)	CNN	PET reconstruction bias -1.72 ± 4.22%	Shiri et al., 2020 ³⁷
Whole body PET (FDG)	CNN	NRMSE 0.21 ± 0.05 SUV, SSIM 0.98 ± 0.01, PSNR 36.3 ± 3.0 dB	Yang et al., 2020 ³⁸
Whole body PET (FDG)	CNN, GAN	MAE of < 110 HU, PET reconstruction bias <1%, PSNR >42 dB	Dong et al., 2019 ¹⁵

Challenges and Opportunities for AI Approaches

The implementation of AI is not without challenges. There are numerous general issues that must be addressed with regards to the application of AI in medical imaging, and many of those issues affect the techniques described herein. Generalization, or the ability of a developed model to be applied to a wide range of input data, and bias, or the tendency of the developed models to favor only certain situations, are important challenges in the field of AI³⁹. For the applications of AI in attenuation and scatter correction, these biases affect the generalizability of a model and are thus critical to understand and address. While bias can be unintentional, it can have significant effects on the performance of models in the field compared to the tightly constrained environment of a research laboratory.

Areas of bias relevant to the techniques described herein are related to the application, population, and equipment used to develop a given AI model. If the model is applied to datasets that differ

greatly in any of these categories, then the model may give spurious outputs that fall outside of the reported performance specifications. An example of application bias would be the use of an AI model for CT synthesis designed for brain imaging being applied to the pelvis. If the model was developed using only brain imaging data, it cannot be expected to perform well in other body regions. Additionally, if the model was trained with a particular MRI sequence but applied using a different MRI sequence, performance may be degraded.

Another source of bias is related to population of which the model is trained and applied to. Patients with different or abnormal anatomy of types that was not included within the training data could cause the model to give unexpected outputs. Therefore, training datasets must incorporate the type of data that is expected to be applied to the model or population specific biases (e.g., female and male, adult and pediatric, implants and amputations) will lead to unpredictable performance of model. There exist many recent demonstrations of this type of bias in AI in popular media outlets.

Finally, the specific equipment used may have a direct impact on the output of a given model. A given model may ultimately be specific to aspects of the equipment from which the images came, including, but not limited to the choice of vendor, site-specific protocols, etc. While this may be advantageous to single medical imaging equipment vendor, the ability of an AI model to be applied to multiple scanner systems is likely to be more impactful and lead to greater standardization of these powerful new methods. The key to enabling greater generalization lies in the development of multi-site and multi-vendor trials, where models are trained on data originating from different sites and equipment from different vendors. The use of federated learning techniques⁴⁰, where training is distributed to different sites, without requiring the transfer of individual images, is gaining traction as a valuable method to reduce site-specific bias and increase generalizability of developed models.

Summary

AI technology holds great promise to improve methods related to quantitative PET and SPECT imaging. The ability of AI-based approaches to obviate the need for an additional CT or transmission image greatly improves the capability of existing equipment and potentially reduces the cost of future

systems. Integrating AI into scatter correction also leads to the ability to improve quantification as well as patient throughput by accelerating these necessary corrections. It can only be expected that these methods will continue to improve in the future and further increase capability.

Clinical Care Points

- Many AI-based approaches to improve attenuation correction for PET and SPECT have been demonstrated in the literature, and will likely make their way to the clinic soon.
- AI-based methods for scatter correction can improve the reconstruction time, potentially improving throughput.
- AI-based approaches can be subject bias based on the data used to train the model. Care should be taken when these methods are applied to different populations and patients with abnormal anatomy for which the AI model has not been trained to utilize.

References

1. Lee TC, Alessio AM, Miyaoka RM, Kinahan PE. Morphology supporting function: attenuation correction for SPECT/CT, PET/CT, and PET/MR imaging. *Q J Nucl Med Mol Imaging Off Publ Ital Assoc Nucl Med AIMN Int Assoc Radiopharmacol IAR Sect Soc Of*. 2016;60(1):25-39.
2. Bailey DL. Transmission scanning in emission tomography. *Eur J Nucl Med*. 1998;25(7):774-787.
3. Watson CC, Casey ME, Michel C, Bendriem B. Advances in scatter correction for 3D PET/CT. In: *IEEE Symposium Conference Record Nuclear Science 2004*. Vol 5. ; 2004:3008-3012. doi:10.1109/NSSMIC.2004.1466317
4. Zaidi H, Montandon M-L. Scatter Compensation Techniques in PET. *PET Clin*. 2007;2(2):219-234. doi:10.1016/j.cpet.2007.10.003
5. Hutton BF, Buvat I, Beekman FJ. Review and current status of SPECT scatter correction. *Phys Med Biol*. 2011;56(14):R85-112. doi:10.1088/0031-9155/56/14/R01
6. Torres-Velázquez M, Chen W-J, Li X, McMillan AB. Application and Construction of Deep Learning Networks in Medical Imaging. *IEEE Trans Radiat Plasma Med Sci*. 2021;5(2):137-159. doi:10.1109/TRPMS.2020.3030611
7. Bradshaw TJ, McMillan AB. Anatomy and Physiology of Artificial Intelligence in PET Imaging. *PET Clin*. Published online This Series.
8. Sorin V, Barash Y, Konen E, Klang E. Creating Artificial Images for Radiology Applications Using Generative Adversarial Networks (GANs) - A Systematic Review. *Acad Radiol*. 2020;27(8):1175-1185. doi:10.1016/j.acra.2019.12.024
9. Lee JS. A Review of Deep-Learning-Based Approaches for Attenuation Correction in Positron Emission Tomography. *IEEE Trans Radiat Plasma Med Sci*. 2021;5(2):160-184. doi:10.1109/TRPMS.2020.3009269

10. Wang T, Lei Y, Fu Y, et al. Machine learning in quantitative PET: A review of attenuation correction and low-count image reconstruction methods. *Phys Medica PM Int J Devoted Appl Phys Med Biol Off J Ital Assoc Biomed Phys AIFB*. 2020;76:294-306. doi:10.1016/j.ejmp.2020.07.028
11. Spadea MF, Maspero M, Zaffino P, Seco J. *Deep Learning-Based Synthetic-CT Generation in Radiotherapy and PET: A Review.*; 2021.
12. Sakaguchi K, Kaida H, Yoshida S, Ishii K. Attenuation correction using deep learning for brain perfusion SPECT images. *Ann Nucl Med*. Published online March 9, 2021. doi:10.1007/s12149-021-01600-z
13. Liu F, Jang H, Kijowski R, Zhao G, Bradshaw T, McMillan AB. A deep learning approach for 18F-FDG PET attenuation correction. *EJNMMI Phys*. 2018;5(1):24. doi:10.1186/s40658-018-0225-8
14. Liu F, Jang H, Kijowski R, Bradshaw T, McMillan AB. Deep Learning MR Imaging–based Attenuation Correction for PET/MR Imaging. *Radiology*. 2017;(September):170700. doi:10.1148/radiol.2017170700
15. Arabi H, Zeng G, Zheng G, Zaidi H. Novel adversarial semantic structure deep learning for MRI-guided attenuation correction in brain PET/MRI. *Eur J Nucl Med Mol Imaging*. 2019;46(13):2746-2759. doi:10.1007/s00259-019-04380-x
16. Gong K, Yang J, Larson PE, et al. MR-based attenuation correction for brain PET using 3D cycle-consistent adversarial network. *IEEE Trans Radiat Plasma Med Sci*. Published online 2020.
17. Blanc-Durand P, Khalife M, Sgard B, et al. Attenuation correction using 3D deep convolutional neural network for brain 18F-FDG PET/MR: Comparison with Atlas, ZTE and CT based attenuation correction. *PLoS One*. 2019;14(10):e0223141. doi:10.1371/journal.pone.0223141
18. Gong K, Yang J, Kim K, El Fakhri G, Seo Y, Li Q. Attenuation correction for brain PET imaging using deep neural network based on Dixon and ZTE MR images. *Phys Med Biol*. 2018;63(12):125011. doi:10.1088/1361-6560/aac763
19. Jang H, Liu F, Zhao G, Bradshaw T, McMillan AB. Technical Note: Deep learning based MRAC using rapid ultrashort echo time imaging. *Med Phys*. Published online May 15, 2018. doi:10.1002/mp.12964
20. Ladefoged CN, Marnier L, Hindsholm A, Law I, Højgaard L, Andersen FL. Deep Learning Based Attenuation Correction of PET/MRI in Pediatric Brain Tumor Patients: Evaluation in a Clinical Setting. *Front Neurosci*. 2018;12:1005. doi:10.3389/fnins.2018.01005
21. Shi L, Onofrey JA, Liu H, Liu Y-H, Liu C. Deep learning-based attenuation map generation for myocardial perfusion SPECT. *Eur J Nucl Med Mol Imaging*. 2020;47(10):2383-2395. doi:10.1007/s00259-020-04746-6
22. Yang J, Shi L, Wang R, et al. Direct Attenuation Correction Using Deep Learning for Cardiac SPECT: A Feasibility Study. *J Nucl Med Off Publ Soc Nucl Med*. Published online February 26, 2021. doi:10.2967/jnumed.120.256396
23. Torkaman M, Yang J, Shi L, et al. Direct Image-Based Attenuation Correction using Conditional Generative Adversarial Network for SPECT Myocardial Perfusion Imaging. *Proc SPIE-- Int Soc Opt Eng*. 2021;11600. doi:10.1117/12.2580922

24. Pozaruk A, Pawar K, Li S, et al. Augmented deep learning model for improved quantitative accuracy of MR-based PET attenuation correction in PSMA PET-MRI prostate imaging. *Eur J Nucl Med Mol Imaging*. 2021;48(1):9-20. doi:10.1007/s00259-020-04816-9
25. Bradshaw TJ, Zhao G, Jang H, Liu F, McMillan AB. Feasibility of Deep Learning-Based PET/MR Attenuation Correction in the Pelvis Using Only Diagnostic MR Images. *Tomogr Ann Arbor Mich*. 2018;4(3):138-147. doi:10.18383/j.tom.2018.00016
26. Torrado-Carvajal A, Vera-Olmos J, Izquierdo-Garcia D, et al. Dixon-VIBE Deep Learning (DIVIDE) Pseudo-CT Synthesis for Pelvis PET/MR Attenuation Correction. *J Nucl Med Off Publ Soc Nucl Med*. Published online August 30, 2018:jnumed.118.209288. doi:10.2967/jnumed.118.209288
27. Armanious K, Hepp T, Küstner T, et al. Independent attenuation correction of whole body [18F]FDG-PET using a deep learning approach with Generative Adversarial Networks. *EJNMMI Res*. 2020;10(1):53. doi:10.1186/s13550-020-00644-y
28. Jonsson J, Nyholm T, Söderkvist K. The rationale for MR-only treatment planning for external radiotherapy. *Clin Transl Radiat Oncol*. 2019;18:60-65. doi:10.1016/j.ctro.2019.03.005
29. Prats J, Larroza A, Oliver S, Rodríguez-Álvarez MJ. PET scatter correction using machine learning techniques. In: *2019 IEEE Nuclear Science Symposium and Medical Imaging Conference (NSS/MIC)*. IEEE; :1-3.
30. Berker Y, Maier J, Kachelrieß M. Deep Scatter Estimation in PET: Fast Scatter Correction Using a Convolutional Neural Network. In: *2018 IEEE Nuclear Science Symposium and Medical Imaging Conference Proceedings (NSS/MIC)*. ; 2018:1-5. doi:10.1109/NSSMIC.2018.8824594
31. Xiang H, Lim H, Fessler JA, Dewaraja YK. A deep neural network for fast and accurate scatter estimation in quantitative SPECT/CT under challenging scatter conditions. *Eur J Nucl Med Mol Imaging*. 2020;47(13):2956-2967. doi:10.1007/s00259-020-04840-9
32. Qian H, Rui X, Ahn S. Deep learning models for PET scatter estimations. In: *2017 IEEE Nuclear Science Symposium and Medical Imaging Conference (NSS/MIC)*. IEEE; 2017:1-5.
33. Dietze MMA, Branderhorst W, Kunnen B, Viergever MA, de Jong HWAM. Accelerated SPECT image reconstruction with FBP and an image enhancement convolutional neural network. *EJNMMI Phys*. 2019;6(1):14. doi:10.1186/s40658-019-0252-0
34. Arabi H, Bortolin K, Ginovart N, Garibotto V, Zaidi H. Deep learning-guided joint attenuation and scatter correction in multitracer neuroimaging studies. *Hum Brain Mapp*. 2020;41(13):3667-3679. doi:10.1002/hbm.25039
35. Yang J, Park D, Gullberg GT, Seo Y. Joint correction of attenuation and scatter in image space using deep convolutional neural networks for dedicated brain 18F-FDG PET. *Phys Med Biol*. 2019;64(7):075019. doi:10.1088/1361-6560/ab0606
36. Mostafapour S, Gholamiankhah F, Dadgar H, Arabi H, Zaidi H. Feasibility of Deep Learning-Guided Attenuation and Scatter Correction of Whole-Body 68Ga-PSMA PET Studies in the Image Domain. *Clin Nucl Med*. Published online March 4, 2021. doi:10.1097/RLU.00000000000003585
37. Shiri I, Arabi H, Geramifar P, et al. Deep-JASC: joint attenuation and scatter correction in whole-body 18F-FDG PET using a deep residual network. *Eur J Nucl Med Mol Imaging*. 2020;47(11):2533-2548. doi:10.1007/s00259-020-04852-5

38. Yang J, Sohn JH, Behr SC, Gullberg GT, Seo Y. CT-less Direct Correction of Attenuation and Scatter in the Image Space Using Deep Learning for Whole-Body FDG PET: Potential Benefits and Pitfalls. *Radiol Artif Intell.* 2021;3(2):e200137. doi:10.1148/ryai.2020200137
39. Kaushal A, Altman R, Langlotz C. Geographic Distribution of US Cohorts Used to Train Deep Learning Algorithms. *JAMA.* 2020;324(12):1212-1213. doi:10.1001/jama.2020.12067
40. Rieke N, Hancox J, Li W, et al. The future of digital health with federated learning. *NPJ Digit Med.* 2020;3:119. doi:10.1038/s41746-020-00323-1
41. Pinykh OS, Langa G, Dewey M, et al. Continuous Learning AI in Radiology: Implementation Principles and Early Applications. *Radiology.* 2020;297(1):6-14. doi:10.1148/radiol.2020200038